CLAS-NOTE 2002-005

Comparison of GSIM Monte Carlo and Geometric Acceptance Functions for CLAS

Matthias U. Mozer, Daniel S. Carman
Ohio University, Athens, OH 45701

March 27, 2002

Abstract

We present a comparison of two different acceptance models for the CLAS detector at Jefferson Laboratory. This note is focused on the reaction $e+p \to e'+K^+ +\Lambda,\ \Lambda \to p+\pi^-$, however, the conclusions to be drawn from this acceptance function comparison are quite general and should be illustrative for all analyses with multiple charged particles in the final state. Two models were compared, the first is a standard Monte Carlo simulation with the GSIM software package, and the second is a geometrical model based on defining fiducial regions of the CLAS in which the geometrical acceptance for individual charged particles can be assumed to be large and uniform. The two models agree in the general trends they show, but the GSIM model exhibits a stronger dependence on the kinematic variables and is sensitive to several subtle but important dependencies on the kinematic variables that the geometric model misses. Ultimately the acceptance function that can be employed is intimately connected with the analysis procedure for a given experiment.

1 Introduction

During the analysis of experiment E99-006 [1, 2], two different methods have been used to determine the CLAS acceptance function. The first technique, referred to as the Geometrical Model, is based on defining a fiducial volume of the CLAS where the detector geometrical acceptance for individual charged particles is large and uniform. With this volume defined, the geometric acceptance of CLAS can be determined on an event-by-event basis even for final states containing multiple charged particles. The second technique to determine the acceptance of CLAS is through the more standard GEANT-based GSIM Monte Carlo approach.

This CLAS-note is designed to compare the results of the two approaches, highlighting the similarities and differences between the two. Clearly the GSIM calculation is expected to represent the superior approach based on its detailed modeling of the CLAS, the fact that the simulation and event reconstruction codes are identical, and due to the inclusion of important effects such as radiation, track reconstruction efficiencies, bad element knock out, and detector efficiency.

From a general viewpoint, the GSIM simulation and the Geometrical Model provide consistent results when analysis methods are used that are insensitive to the details of the acceptance function, such as in the measurement of cross section asymmetries. However, for other analyses, such as measurement of a cross section, the Geometrical Model misses several more subtle but important dependencies of the acceptance function on the kinematic variables.

This note will focus specifically on comparisons of the acceptance calculations for the specific final state of interest in E99-006, namely $e + p \rightarrow e' + K^+ + \Lambda,\ \Lambda \rightarrow p + \pi^-$. However, the conclusions to be drawn from this comparison are quite general and should be illustrative for all analyses with multiple charged particles in the final state.

The main reason for investigating alternative approaches to GSIM for calculation of the acceptance function of CLAS is the nearly prohibitive amount of CPU time required for the task. The acceptance tables must be generated in the required number of kinematic variables, with sufficiently small bin sizes and acceptable statistical errors for each different beam energy / torus field setting of the data set. For the final state of E99-006 where three charged particles are detected, namely the e', K^+, and p (π^- missing), the typical acceptance is on the order of 5%. To fully define the kinematics at a given beam energy for each event, we define the acceptance in terms of the following six quantities:

Q^2**:** Four-momentum transfer squared ($q = p_e - p_{e'},\ Q^2 = -q^2$).

W**:** Invariant energy in the resonance center-of-mass frame.

θ_K^{cm}**:** Polar angle of the kaon in the resonance center-of-mass frame.

ϕ_K^{cm}**:** Relative angle between the electron scattering plane and the $K - \Lambda$ scattering plane.

θ_p^{RF}**:** Polar angle of the Λ decay proton relative to the spin-quantization axis in the hyperon rest frame.

ϕ_p^{RF}**:** Azimuthal angle of the Λ decay proton in the hyperon rest frame.

For this study we employed the 4.247 GeV/2250 A data set from the e1c running period. The binning employed is given in Table 1. With our six variables, even with the very coarse binning employed, we require roughly 100-200M Monte Carlo events for each beam/torus setting to achieve statistical uncertainties on our acceptance calculation at the level of $\leq$20% in each of our 52500 bins.

Variable	Range	N_{bins}
Q^2	$0.9 \rightarrow 2.5$ (GeV/c)^2	7
W	$1.6 \rightarrow 2.5$ GeV	5
$\cos\theta_K^{cm}$	$-1.0 \rightarrow 1.0$	6
ϕ_K^{cm}	$-\pi \rightarrow \pi$	10
$\cos\theta_p^{RF}$	$-1.0 \rightarrow 1.0$	5
ϕ_p^{RF}	$-\pi \rightarrow \pi$	5

Table 1: Number of bins chosen in each of our kinematic variables for the acceptance function comparison.

For the e1c data set of 1999, there are six different combinations of beam energy / torus current that are being analyzed. Our experience with using the CPU farms at Jefferson Laboratory and Ohio University indicate the we can generate and reconstruct (i.e. cook) roughly 2-3M Monte Carlo events per day. Thus the number of days to generate the very coarse acceptance tables, fully within our statistical uncertainty limits, would amount to roughly 1-2 years! Clearly seeking out a practical alternative can drastically reduce the analysis period.

2 Acceptance Calculations

2.1 Geometrical Model

When studying acceptance corrections, it is convenient to divide the problem between the effects related to the geometrical acceptance and those related to the efficiency of the detector and the offline analysis (e.g. track reconstruction efficiencies). The geometrical acceptance issue can be solved in a straightforward manner because fiducial cuts have been used in the analysis. These fiducial cuts, defined separately for both the electron and hadrons, determine a precise geometrical region of the detector where events are accepted. These fiducial cuts are specifically designed to eliminate the low efficiency areas of the CLAS acceptance near the coils of the torus. A plot of these fiducial cuts in terms of laboratory angles is shown in Fig. 1. The functional form of the employed fiducial cuts is included in the Appendix.

The geometrical acceptance within the fiducial region can be calculated and used to apply an acceptance correction to the data on an event-by-event basis. This procedure was initially developed by Raffaella DeVita for the analysis of the EG1 double-spin asymmetries [3]. Of course, the acceptance function determination is more complicated for the present analysis due to the nature of the three-body final state.

The Geometrical Model represents an analytic approach to determining the acceptance for our three-body final state. The final acceptance determined for the event represents

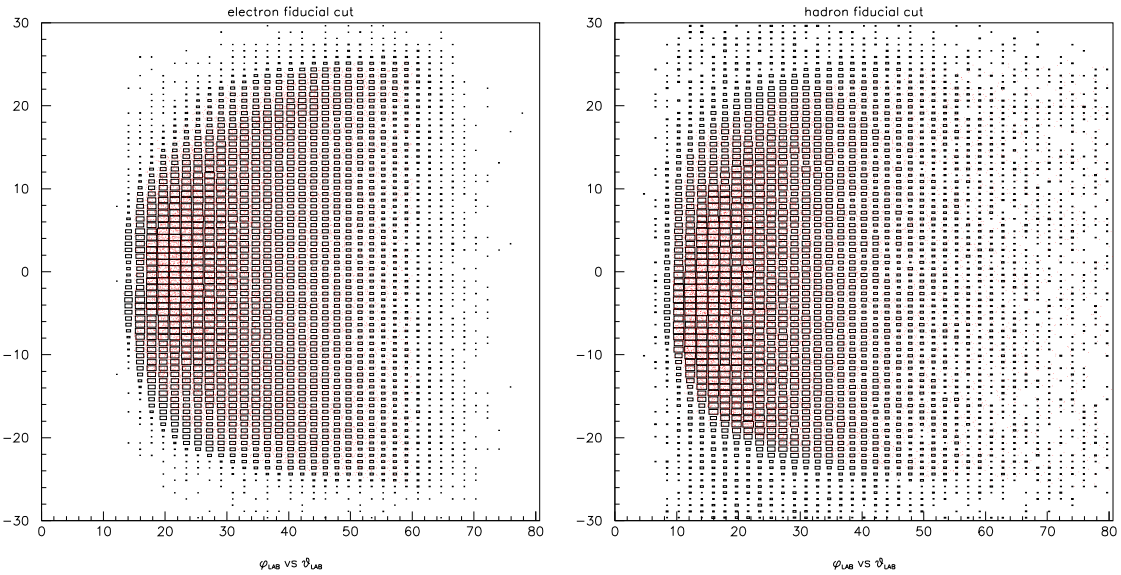

Figure 1: Plot of laboratory ϕ vs. θ (deg) showing the angular distribution of detected electrons and hadrons before (black) and after (red) the fiducial cuts have been applied. The picture can only give a rough impression of the cuts as they are momentum dependent.

the convolution between the three functions that define the fiducial regions separately for the final state electron, kaon, and proton [2]. Fig. 2 illustrates the procedure for a typical event. This figure schematically shows the six CLAS sectors as the solid outlines. The dashed outlines represent the fiducial cuts that are used to define the precise geometrical acceptance. This definition fixes the ϕ extent of each sector as a function or θ for both electrons and hadrons. In the analytical calculation, the measured event in CLAS determines the specific values for the laboratory angles θ_e, θ_K, θ_p, $\Delta\phi_{eK}$, and $\Delta\phi_{pK}$.

The first step of the calculation is to allow the electron to have all values of ϕ within the defined electron fiducial cuts at the measured value of θ_e for one sector. This is shown as the shaded region between points A and B in Fig. 2. From the measured value of $\Delta\phi_{eK}$, the ϕ range of the associated kaon is therefore fixed between the limits of C and D. The accepted range of ϕ_K for an event with this kinematics is then the shaded region between points C and D, or that ϕ range within the fiducial region for positively charged hadrons. For each portion of this ϕ range that is within the fiducial volume of CLAS, the range of ϕ for the associated decay proton is studied. This range is fixed by the value of $\Delta\phi_{pK}$ for the event and must lie between the limits of E and F. The shaded region between points E and F is called $\delta\phi_3$. This calculation is repeated for the electron in each of the six CLAS sectors. The geometrical acceptance assigned to this event, with its given kinematics, is then given by:

$$\mathrm{GACC} = \frac{\sum_{i=1}^{6} \delta\phi_3}{2\pi}. \tag{1}$$

In this procedure, we explicitly check whether any of the final state particles fall onto a known bad scintillation counter as we rotate through ϕ. Azimuthal angle ranges where this occurs are not included within the $\delta\phi_3$ sum.

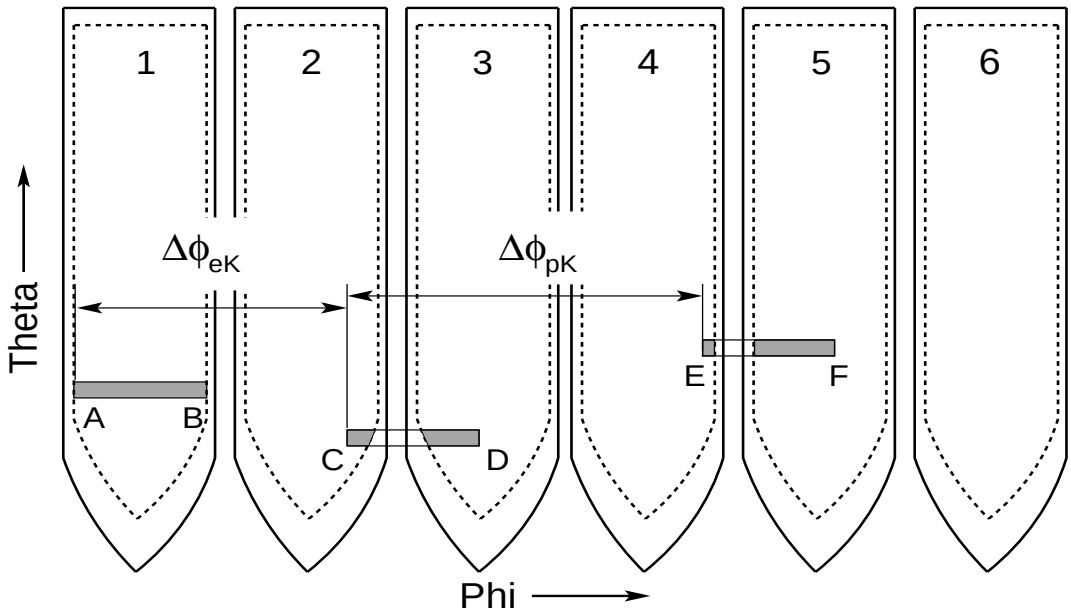

Figure 2: Schematic picture of CLAS to illustrate how the geometrical acceptance is calculated for each event.

Our Geometrical Model also includes a factor to account for the kaons that are lost due to in-flight decay. The calculated acceptance for the event is multiplied by the kaon survival probability K_{sp}:

$$K_{sp} = \exp\left(\frac{-m_K L_K}{\tau_K p_K}\right). \tag{2}$$

Here L_K is the kaon path length from the target to the outer scintillation counters, m_K is the kaon mass, p_K is the kaon momentum, and τ_K is the proper lifetime of the kaon ($c\tau_K = 3.713$ m [4]). This survival probability is shown in Fig. 3 as a function of kaon laboratory polar angle.

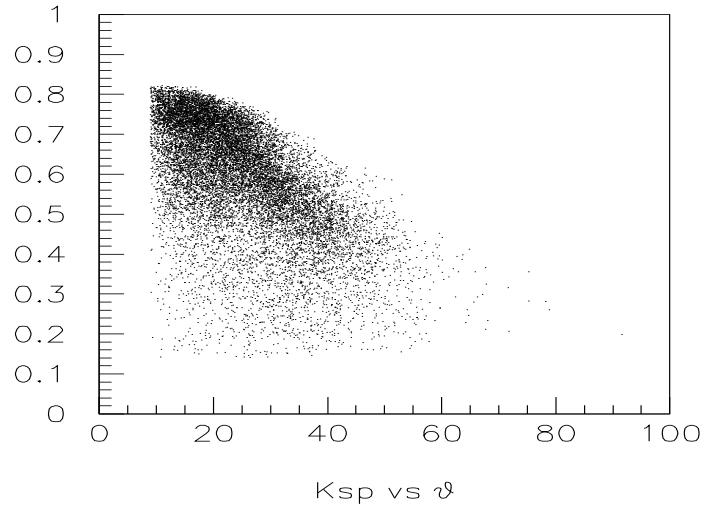

Figure 3: The K^+ survival probability in CLAS from the target to the scintillation counters as a function of the kaon laboratory scattering angle (deg).

Finally, the expression for acceptance also includes a factor for the Λ decay branching ratio to the $p\pi^-$ final state of 0.64. Thus the acceptance for each event in our Geometrical Model is given by:

$$\mathrm{ACC} = \mathrm{GACC} \cdot 0.64 \cdot K_{sp}. \tag{3}$$

The weighting factor assigned to the event histogram is then simply 1/ACC. The average three-body acceptance is on the order of 5%. The distribution of the weights for a typical data set at a beam energy of 4.247 GeV and a torus current of 2250 A is shown in Fig. 4. The events that have a weight of zero assigned to them include at least one particle that does not lie within the defined fiducial volume.

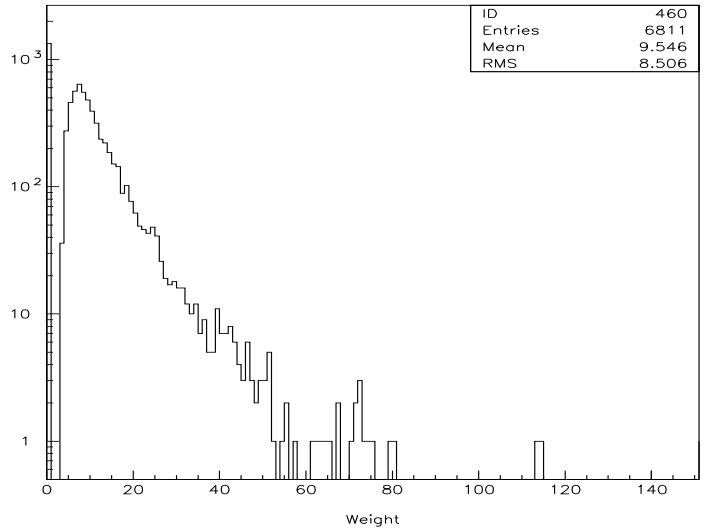

Figure 4: Distribution of the weights from the geometric acceptance model for E_b=4.247 GeV and I_t=2250 A.

The relative simplicity of this approach is countered in some respects by the fact that several important details of the CLAS response that affect the acceptance function are not explicitly considered. These effects include:

- Bad or missing drift chamber (DC) channels
- Missing electromagnetic calorimeter (EC) channels
- Čerenkov counter efficiency map
- Track reconstruction efficiency
- Track correlation effects
- Radiative effects for electrons and hadrons
- Bin migration

2.2 GSIM Monte Carlo Model

For the GSIM model the standard GEANT-based software was used with slight modifications. The events were generated with *RadGen* [5], setting the beam energy to 4.247 GeV and the torus / mini-torus current to 2250 / 6000 A. Two different models for the cross section were employed: a phase-space distribution and a model devised by T. Mart [6]. Ideally one would like to use a cross section model that is very close to the real cross section to be less sensitive to the effects of bin migration. But the more realistic cross section model produced only very few events in some kinematic regions. To bring the statistical error of the acceptance function in these regions to an acceptable value with a moderate amount of CPU time, it was necessary to include events from the phase-space generator to better cover these kinematic regions. The events were then simulated with GSIM and additional smearing was introduced with the GSIM post-processor *gpp*, which also introduced the signatures of bad scintillator paddles and dead DC wires. The resulting Monte Carlo data was processed with the same software as was used for the cooking of the original e1c data (*a1c* version 1-9). The program to convert the resulting *.bos*-file output into Ntuples (*nt10maker*) had to be modified to extract the simulated 4-momenta for the decay products of the Λ hyperon. The Ntuples were then processed with nearly the same analysis code that was used to analyze the original data.

Several changes had to be introduced into the analysis code because GSIM does not yet fully model all parts of the detector response. The first modification was to include the Čerenkov counter efficiency function devised by Alex Vlassov [7]. Each event was assigned an efficiency according to the position of the electron track on the face of the Čerenkov counter. Events were randomly removed, with the chance of removal being the inverse of the efficiency assigned to the event. Additionally, the RF-timing information that is provided by GSIM does not match the real signal, so that we were not able to calculate the mass of the particles from the timing information, as it is done for real data. Instead the hadron mass values from the SEB banks [8] were used.

3 Acceptance Function Comparison

To compare the two acceptance calculations, we applied both models to data that was taken at E_b=4.247 GeV, I_t=2250 A, and I_{mt}=6000 A. Fig. 5 shows the acceptance functions according to the two models, integrated over all but one of our kinematic variables. These plots highlight the general trends of the acceptance function, but the integration hides many details that can only be seen if the acceptance is studied as a function of more than one variable. Fig. 6 shows the acceptance as a function of W and the angle coordinates.

Firstly it has to be noted that the acceptance calculated with the Geometrical Model is, in general, about three times as high as that resulting from GSIM. This is due to several contributions that have been omitted in the Geometrical Model for simplicity. The main factors include the Čerenkov counter efficiency, the reconstruction efficiency, and radiative effects.

The effect of the Čerenkov counter efficiency was estimated to reduce the acceptance by a factor of about 1.5 by looking at Monte Carlo data with and without the Čerenkov counter

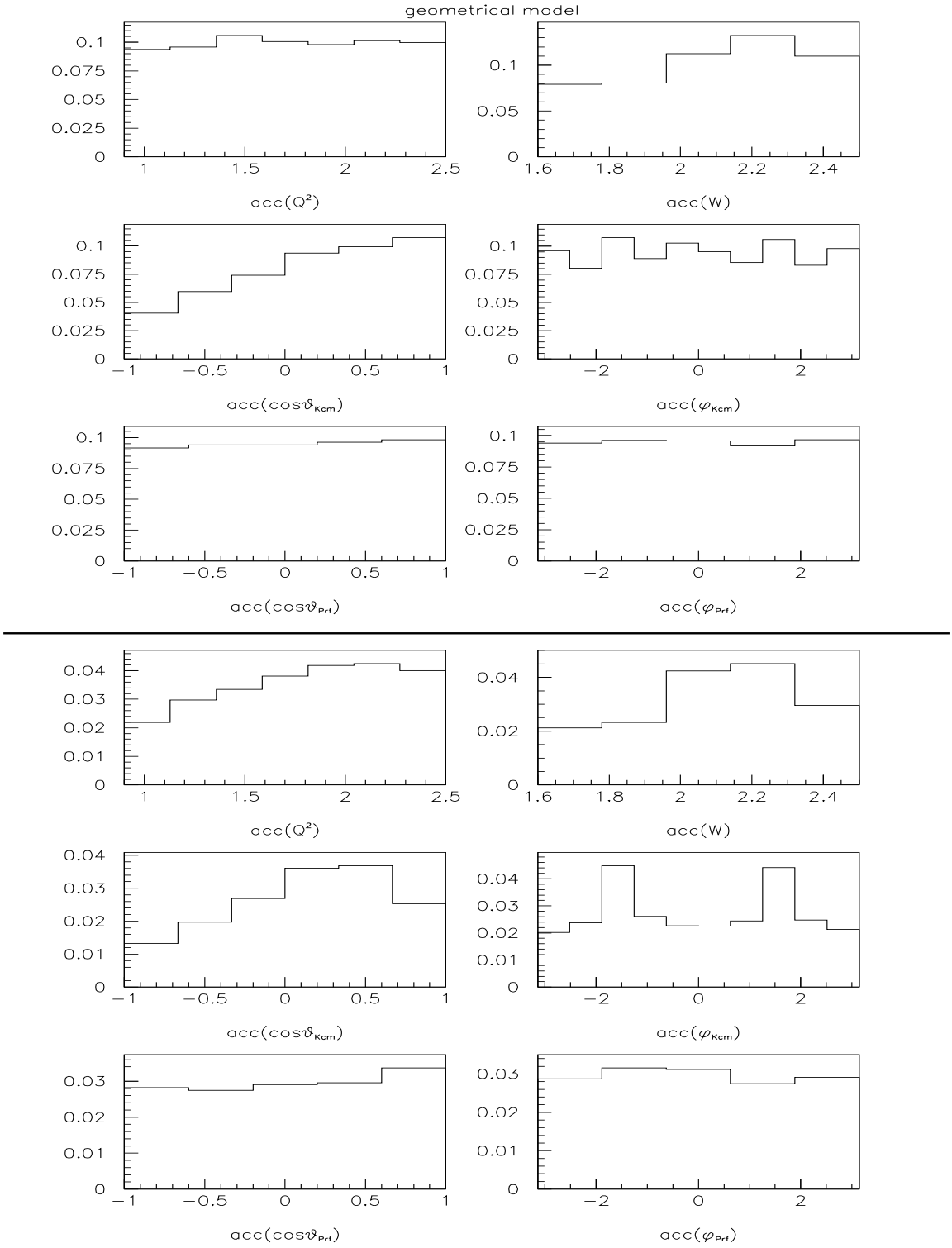

Figure 5: The acceptance integrated over all but one variable for the Geometrical Model (upper plots) and the GSIM model (lower plots) applied here to data with E_b=4.247 GeV, I_t=2250 A, and I_{mt}=6000 A.

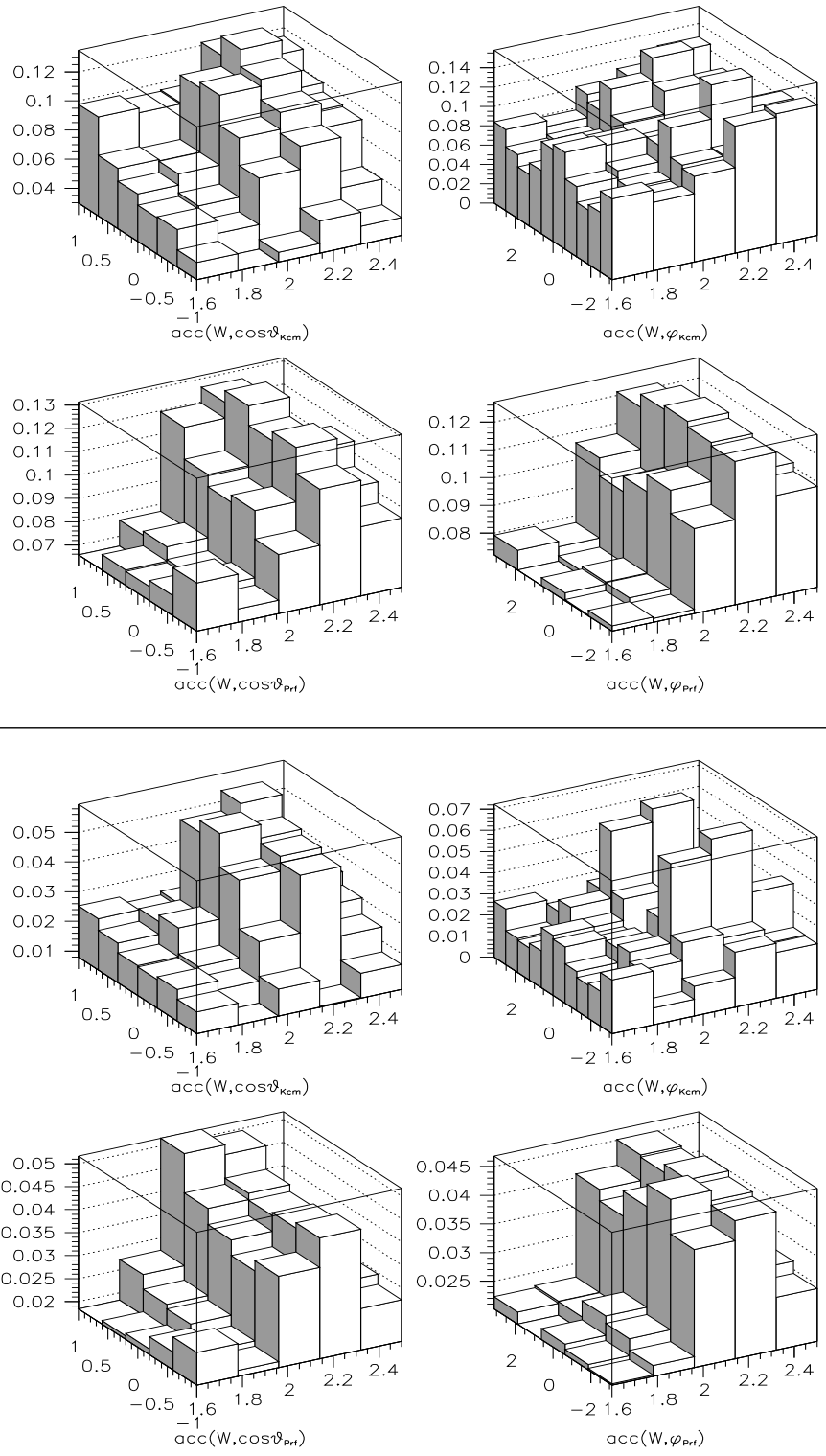

Figure 6: The acceptance integrated over all variables but W (front scale) and one angle (side scale) for the Geometrical Model (upper plots) and the GSIM model (lower plots) applied here to data with E_b=4.247 GeV, I_t=2250 A, and I_{mt}=6000 A.

efficiency correction turned on. The reconstruction efficiency includes several different effects that all lower the number of events that are successfully reconstructed by the analysis program. These include events that cannot be reconstructed due to missing EC channels and DC wires. Although the inefficiency for single tracks in a sector is only at the few percent level (∼4%, including dead EC and DC channels), the analysis code has a significantly lower chance of correctly reconstructing an event if two of the tracks are contained within a single sector and are relatively close to each other (see [9]). In our data sample about one quarter of the kaons and decay protons are detected in the same sector, while the electron and one of the hadrons (kaon or decay proton) occupy the same sector only in a few percent of all cases (see Fig. 7). For the hadron momentum differences involved in our data, the reconstruction efficiency is ∼80-90% when both hadrons lie in the same sector, implying a total loss of acceptance of a ∼4%.

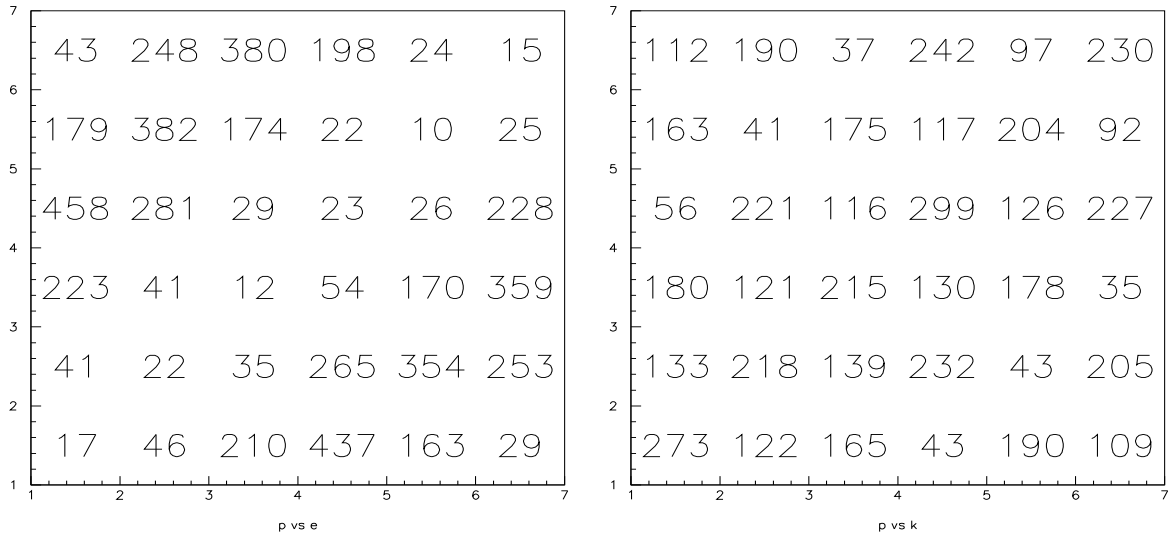

Figure 7: Number distributions of electron sector vs. proton sector (left) and proton sector vs. kaon sector (right) showing where the final state particles were reconstructed in a representative data sample. The plot for the kaon/electron correlation (not shown here) is very similar to the proton/electron plot.

The radiative effects have two main consequences for the acceptance. First, events that contain a Bremsstrahlung photon tend to be reconstructed at a higher W than they really had (see Fig. 8). Second, radiative effects will, in general, induce errors in the missing-mass calculation, causing the so-called "radiative tails" in the missing-mass distribution. The cuts on the missing mass that have been introduced into the analysis code to suppress background will also remove many events that have undergone radiation. Turning the radiative effects in the GSIM model on and off lets one estimate this general loss of events (and hence reduction in acceptance) to be roughly 30%. This contributes further to the large discrepancy in average acceptance between the two models.

Further the bin migration has to be considered. The Monte Carlo model accounts for the events that are produced in the kinematic region under investigation but are reconstructed outside of it for various reasons. The Geometrical Model can not correct for these losses, but it turns out that the loss due to bin migration is less than 1% and thus plays a negligible

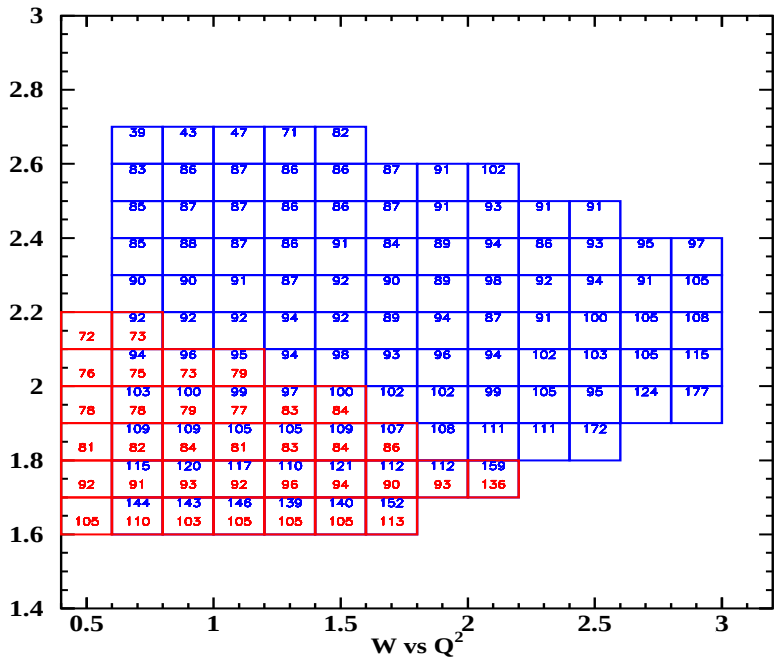

Figure 8: W and Q^2 dependence of the radiative correction factors for E_b=4.247 GeV (blue/upper value) and E_b=2.567 GeV (red/lower value). The correction factor shows what percentage of the events in each bin would occupy this bin if radiation did nor occur. This graph was created by Gabriel Niculescu for the analysis of experiment E93-030 [10].

role compared to the other factors for the average acceptance. Taking all these effects into account, the average acceptance for the two models still differs by ∼25%. The remaining difference is discussed in Section 4.

The second general difference between the two acceptance models is that the GSIM results show a stronger dependence on the kinematic variables than the Geometrical Model does. When one compares the two models variable by variable, one can first see that the Q^2 dependence of the GSIM acceptance is quite strong, while the Geometrical Model is relatively flat in this variable. This effect arises due to the Čerenkov counter efficiency that depends strongly on the polar scattering angle of the electron (see [7]). This effect can be seen in Fig. 9 which demonstrates that Q^2 is strongly correlated with θ_e. The Čerenkov counter has a region of low efficiency at small angles (see Fig. 10). Therefore, including the Čerenkov counter efficiency in the Monte Carlo model will lower the acceptance for small electron polar angles and thus for low Q^2. One could counter this drawback of the Geometrical Model by applying fiducial cuts that allow electrons only within the region of high Čerenkov counter efficiency, but the enormous loss of statistics and kinematic coverage makes this impractical. The radiative corrections on the other hand do not depend strongly on Q^2 (see Fig. 8), and thus cannot be responsible for the difference in the Q^2 dependence.

The distribution of the acceptance in W seems to be in reasonable agreement between the two models. Except for the bin with the most forward angle, the distributions in $\cos\theta_K^{cm}$ are likewise comparable. The lowering of the acceptance with increasing θ_K^{cm} can be explained in the following way. A large θ_K^{cm} corresponds to a large angle of the kaon in the laboratory frame. The kaons with large angle typically have lower momenta, so that some of them decay

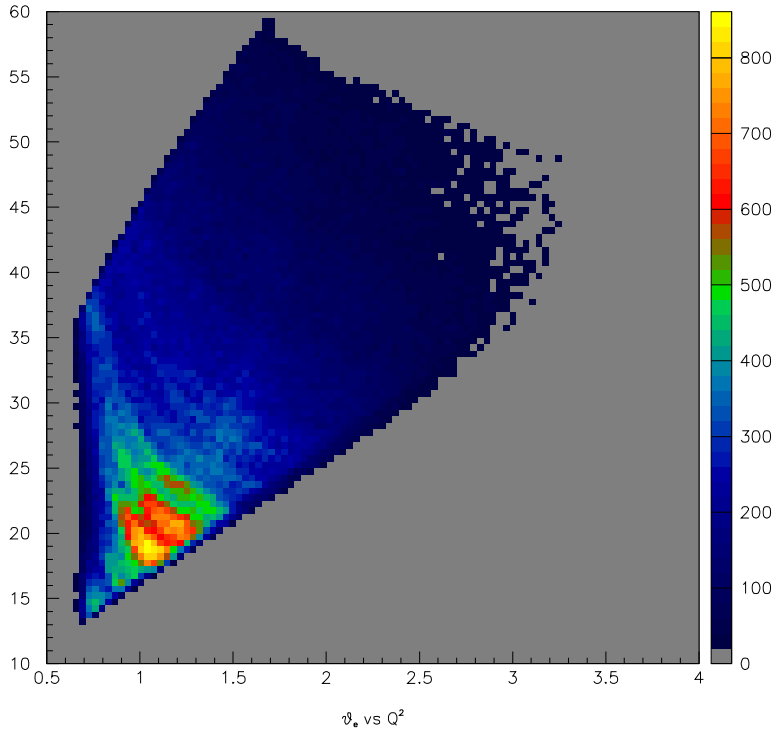

Figure 9: The correlation between the electron laboratory polar angle θ_e (deg) and Q^2 ((GeV/c)^2) at 4.247 GeV/2250 A.

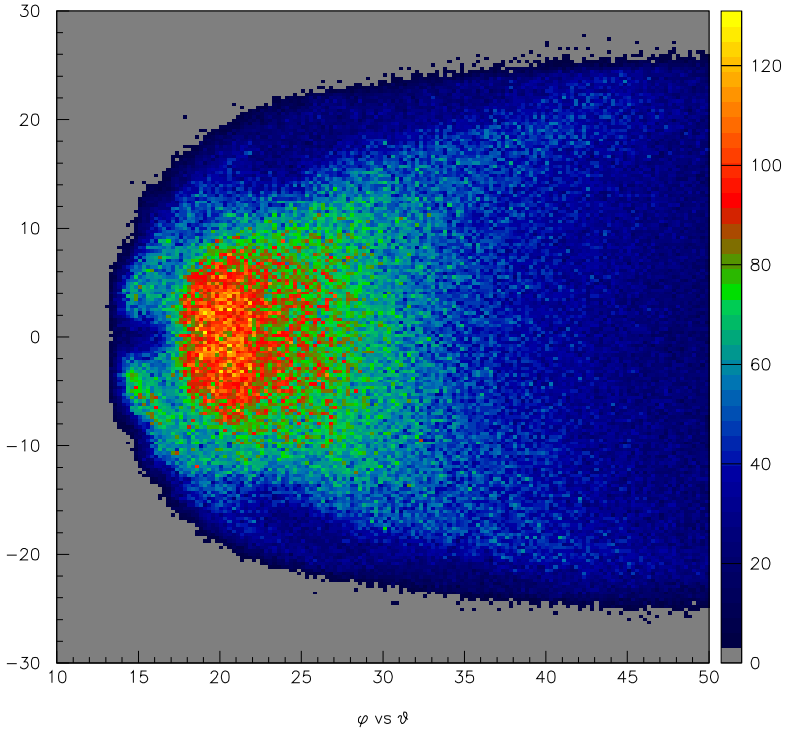

Figure 10: The distribution of the scattered electrons summed over all six sectors in terms of laboratory ϕ_e vs. θ_e (deg) at 4.247 GeV/2250 A .

before they can pass through all three drift chamber regions of CLAS and reach the outer scintillation counters. The fall off in the GSIM model is steeper as this model also takes into account that low momentum kaons can curl up in the magnetic field and thus escape detection.

For the dependence of the acceptance on the angle between the hadron and the electron planes, ϕ_K^{cm}, one would, on first thought, expect a six-fold symmetry caused by the six coils of CLAS. This is somewhat washed out by the low number of bins. The cause of the strong W dependence of the acceptance in ϕ_K^{cm} is the strong correlation between W and the opening angle between the kaon and the decay proton. This angle distribution, convoluted with the acceptance holes in CLAS due to the coils, accounts for the acceptance that can be seen in Fig. 6. The difference in amplitude between the variations in the acceptance with ϕ_K^{cm} in the two models can partly be traced back to the Čerenkov counter efficiency. The Čerenkov counter has a region of low efficiency near the coils (see Fig. 10) that causes the two peaks in the ϕ_K^{cm} acceptance to be more pronounced. This effect can be mimicked in the Geometrical Model by introducing very narrow fiducial cuts that simulate the low Čerenkov counter efficiency near the coils. As these narrow cuts cause a loss of data unacceptable from a statistical point of view, they were only applied for test purposes. A further contribution to the discrepancies lies in inadequacies of the cross section models that were used to generate the Monte Carlo data. Applying the Geometrical Model to a sample of the Monte Carlo data shows differences in the ϕ_K^{cm} acceptance for the two different cross section models that were used (phase space distribution and code by T. Mart [6]). Ideally one would like to only use the more realistic cross section model to produce a more accurate result, but this cross section model tends to populate some kinematic regions only very sparsely; we therefore had to rely on a phase-space distribution to achieve sufficient statistical accuracy in these regions, thus introducing further uncertainties.

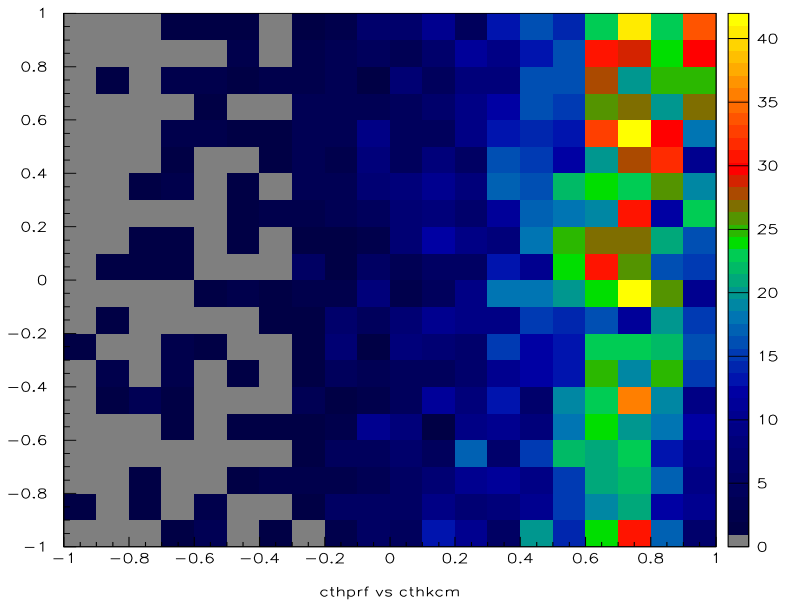

Figure 11: Plot of $\cos\theta_p^{RF}$ vs. $\cos\theta_K^{cm}$ for W between 2.14 GeV and 2.32 GeV at 4.247 GeV/2250 A.

The dependence of the acceptance as a function of the decay proton angles θ_p^{RF} and

ϕ_p^{RF} is difficult to interpret, mainly because there is no intuitive connection between these variables and the track positions in the lab frame, although the two models agreement here. The slightly higher acceptance for forward θ_p^{RF} angles can be explained in terms of the weak correlation between θ_p^{RF} and θ_K^{cm} (see Fig. 11). The correlation varies with W, which explains why the effect of this correlation is washed out when integrated over W (compare Fig. 5 and Fig. 6). The acceptance in the azimuthal decay proton angle ϕ_p^{RF} is comparatively flat in both models. In the GSIM model the acceptance has been integrated over ϕ_p^{RF}, so that one should expect this part of the acceptance to be rather flat.

4 Event Weight Comparison

To check whether the agreement between the two models is not just superficial, the weights assigned to the real data events can be compared event for event (see Fig. 12). The result of this study is that, in general, both models agree reasonably well, especially where the acceptance is larger. However for larger weights (lower acceptances) the two begin to disagree. One reason here could be that for the low acceptance bins, the statistical error for the acceptance function can be quite large (see Fig 13). However, the spread in the weight differences between the Geometrical Model and the GSIM calculation are more strongly attributable to kinematic-dependent efficiencies that are not included in the Geometrical Model. This arises as events with similar weights can have very different kinematics.

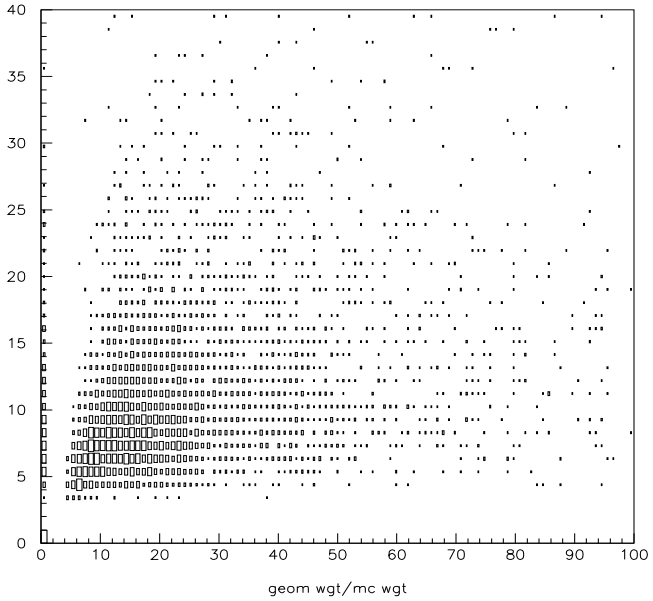

Figure 12: Comparison of the weights assigned by the different acceptance models to events of the real data at 4.247 GeV/2250 A.

Additional discrepancies can be expected between the two acceptance calculation approaches due to inadequacies of the Geometrical Model, especially near the edges of the kinematic and geometrical acceptance of CLAS. Beyond the effects explicitly considered in Section 2.1 in detail, any other loss mechanisms, either due to reconstruction algorithms,

detector response, detector solid angle, etc., only serve to reduce the GSIM calculated acceptance relative to the Geometrical Model. These effects most likely address the unaccounted for 25% discrepancy alluded to in Section 3.

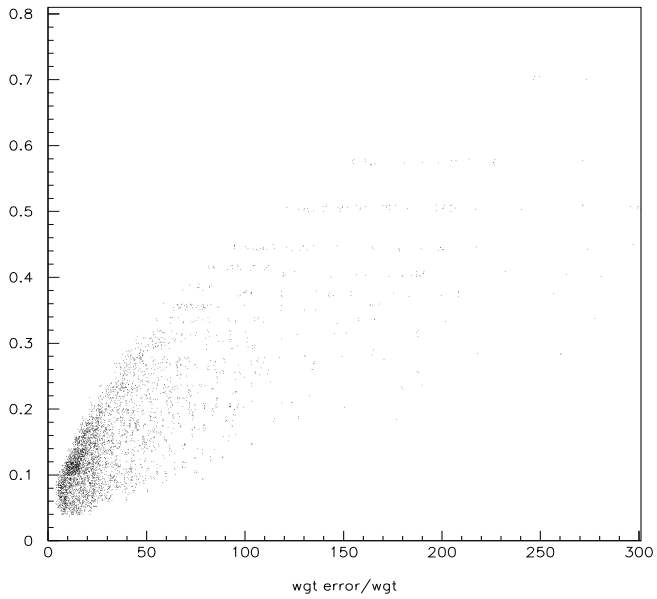

Figure 13: Relative statistical error of the GSIM Monte Carlo acceptance sorted by weight.

5 Weaknesses Of The GSIM Model

The GSIM Monte Carlo method has to struggle with several problems that are not easily overcome. When a realistic cross section is used to generate the initial events, there are extremely few events in the region of low W and higher Q^2. This forces one either to generate enormous amounts of data or to include some fraction of events from a phase-space distribution (which has been done here). The first option would in principle give more accurate results (bin migration would have less influence on the results) but is impractical from the standpoint of CPU time.

The fact that the generated Monte Carlo events are differently distributed than the real data motivates a very close look at bin migration. As a complete migration matrix would be much too large, one matrix for each kinematic variable was generated for our studies. Bin migration was found to occur at the few percent level in all of our kinematic variables. However, depending on the precision desired in the acceptance function, this could force one to rely entirely on a realistic cross section model for the generation of the Monte Carlo data. As the model we used tends to populate some kinematic regions only very sparsely, one would have to invest large amounts of CPU time to gather enough statistics in the disfavored kinematic regions. Additionally, it also proved impractical to produce a fully differential acceptance table. In order to reduce the statistical uncertainty in the GSIM acceptance function to acceptable levels (i.e. $\lesssim$20% for these studies), we opted to integrate our acceptance function over one of our kinematic variables: ϕ_p^{RF}. Only the integration over

one of the kinematic variables made it possible to guarantee reasonable statistical errors in the acceptance function, even in the sparsely populated regions of the kinematics.

A related problem is that the binning of our GSIM acceptance function is much coarser than would be desirable. Especially for variables that strongly affect the acceptance like ϕ_K^{cm}, the number of bins chosen in this analysis are the bare minimum. Unfortunately any increase in the number of bins would further increase the amount of CPU time necessary to guarantee an acceptable statistical accuracy.

One additional uncertainty comes from the calculation of the Čerenkov counter efficiency (see [7]). Unfortunately there was not enough data to properly define the efficiency for some peripheral parts of the counter. Most of the events that lie in these regions are eliminated by the fiducial cuts. For the other events the efficiency was arbitrarily assumed to be zero. This is presumably caused by the fact that there occur too few real events in these regions to properly define the efficiency function. So one can expect that only a few events will be weighted by an acceptance that has been influenced by the undefined Čerenkov counter efficiency.

6 Conclusion

Two approaches for generating an acceptance function for CLAS have been compared, a Geometrical Model that is based on defining fiducial volumes and a standard GSIM simulation. The GSIM model includes more details than the Geometrical Model and shows a stronger dependence on the kinematic variables than the Geometrical Model. The major differences between the two models can be explained in terms of the different level of detail included in each model. In principle the GSIM simulation is preferable to the analytic approach, but practically a Monte Carlo simulation of sufficient quality needs very large amounts of CPU time.

Our studies show that the less work and CPU-intensive Geometrical Model still yields acceptable results if the concerned analysis is not strongly sensitive to the acceptance function (e.g. asymmetry measurements). In analyses sensitive to the acceptance function a full scale GSIM Monte Carlo study is required.

7 Appendix

For the electron the CLAS acceptance is determined mostly by the limits of the ϕ_e acceptance in each sector. The ϕ_e limits are determined by the drop in collection efficiency of the Čerenkov detector mirrors. Fiducial cuts in ϕ_e for electrons are empirically chosen to avoid regions of very low efficiency. The expressions that determine the electron fiducial region for each CLAS sector are given by:

$$\delta\phi_e = \phi_0 \sin(\theta - \theta_{min})^x, \qquad x = a(p_e I_{max}/I)^b$$
$$\theta_{min} = \theta_1 + \theta_2/[(p_e + p_0)I_{max}/I].$$

Here I_{max}/I represents the ratio of the torus current settings relative to $I_{max} = 3375$ A. The minimum scattering angle, θ_{min}, is a function of momentum for the inbending electrons. The parameters θ_1 and θ_2 employed for the electron fiducial cuts are contained in the Table 2. This form for the electron fiducial cuts was inspired by that employed by Cole Smith for the π^0 analysis [11].

E_{beam}/I_{torus}	ϕ_0	θ_1	θ_2	p_0 (GeV/c)	a	b
$\geq$ 4.0 GeV/2250 A	26.0°	8.4°	30.4°	0.287	0.05	1.1
$\geq$ 4.0 GeV/3375 A	26.0°	8.0°	30.4°	0.420	0.05	1.2

Table 2: List of parameters employed in the analysis for the electron fiducial cuts.

For the charged hadrons in this analysis, K^+ and p, the CLAS fiducial cuts are designed to exclude regions of non-uniform acceptance from attenuation due to interactions with the mini-torus coils, the torus cryostat, or from the edges of the drift chamber acceptance. These regions have been assumed to be the same for both kaons and protons, and have the same definition in all CLAS sectors. The expressions that define these fiducial cuts are symmetric about the sector midplane and are given by:

$$\begin{aligned} \delta\phi_h &= \phi_0 \sin(\theta - \theta_{min})^x \\ x &= b(p_h I_{max}/I)^b. \end{aligned}$$

The parameters employed for the hadron fiducial cuts are contained in Table 3.

E_{beam}	ϕ_0	θ_{min}	a	b
$\geq$ 4.0 GeV	26.0°	10.0°	0.15	0.25

Table 3: List of parameters employed in the analysis for the hadron fiducial cuts.

References

[1] D.S. Carman, K. Joo, and B.A. Raue, "Polarization Observables in $p(\vec{e}, e'K^+)\vec{Y}$", Jefferson Laboratory experiment E99-006.

[2] D.S. Carman and B.A. Raue, E99-006 CLAS Analysis Report, in preparation, (2002).

[3] R. DeVita and M. Anghinolfi, "Measurement of Spin Asymmetries in π^+ Electroproduction Using CLAS Data", CLAS Analysis Report, (2001).

[4] C. Caso *et al.*, Rev. of Particle Physics, Eur. Phys. J **C3**, 1 (1998).

[5] RadGen, Event generator program for $ep \to e'X$ written by R.A. Thompson and modified by R. Feuerbach.

[6] H. Haberzettl, C. Bennhold, and T. Mart, Nucl. Phys. **A684**, 475 (2001).

[7] A. Vlassov, Čerenkov efficiency function, see web page for details: http://www.jlab.org/∼vlassov/cc/cc_e1b_eff/e1b_1500.html.

[8] SEB - Simple Event Builder, written by S. Stepanyan.

[9] K. Mikhailov, A. Stavinskiy, and A.Vlassov, CLAS-note 2002-002: "Methods for Close-Track Efficiency Study and its Application for CLAS", (2002).

[10] G. Niculescu, E93-030 CLAS Analysis Report, in preparation, (2002).

[11] L.C. Smith and K. Joo, "Measurement of $p(e, e'p)\pi^0$ Using CLAS", CLAS Analysis Report, (2001).